JOURNAL OF THERMOPHYSICS AND HEAT TRANSFER
Vol. 20, No. 4, October–December 2006

Design Graphs for Thermal Contact Conductance of Similar and Dissimilar Light Alloys

M. A. Lambert*
San Diego State University, San Diego, California 92182-1323
S. R. Mirmira†
Applied Materials Corporation, Santa Clara, California 95054-3299
and
L. S. Fletcher‡
Texas A&M University, College Station, Texas 77843-3123

An extensive set of graphical solutions is presented for thermal contact conductance of similar and dissimilar pairings of three light metals (i.e., aluminum alloy 6061-T6, magnesium alloy AZ31B, and titanium alloy Ti-6Al-4V) widely used in aerospace applications. This graphical format greatly simplifies the process of making estimates of conductance. The plots encompass wide ranges of surface size (2 to 20 cm diameter), roughness (0.1 to 10 μm), and nonflatness (1 μm to 1 mm). The graphs were generated from a model developed by Lambert and Fletcher which compares favorably to the majority of 1265 experimental conductance results from the literature. Herein, the model has been revised, making it simpler and more accurate. A brief derivation of the model is included. Instructions on how to interpret the graphs are provided, as well as practical considerations in using and applying them. The model is compared to new conductance data for similar and dissimilar contacts of the three aforementioned alloys.

Nomenclature

A_{app}	=	apparent contact area, m^2
a_L	=	macrocontact radius for rough spheres, m
$a_{L,\text{Hz}}$	=	Hertz macrocontact radius for smooth spheres, m
a_S	=	radius of microcontact, m
b_L	=	radius of surfaces in contact, m
b_S	=	radius of heat flux channel for microcontact, m
E	=	modulus of elasticity, N/m^2
E'	=	effective elastic modulus, N/m^2, $E' = [(1-\nu_1^2)/E_1 + (1-\nu_2^2)/E_2]^{-1}$
H_C	=	contact microhardness, N/m^2
H_K	=	Knoop microhardness, N/m^2
H_V	=	Vickers microhardness, N/m^2
$h_{C,S+L}$	=	thermal contact (solid spot) conductance, W/m$^2\cdot$K, $1/(R_{C,S}+R_{C,L})$
h_g	=	gap fluid conductance, W/m$^2\cdot$K
h_{junc}	=	junction thermal conductance, W/m$^2\cdot$K, $h_g + h_{\text{rad}} + h_c$
h_{rad}	=	radiative conductance, W/m$^2\cdot$K
J_0, J_1	=	Bessel functions of the first kind
k	=	harmonic mean thermal conductivity, W/m$\cdot$K, $2k_1k_2/(k_1+k_2)$
L	=	contact load, N
L^*	=	dimensionless contact load, $2L/[\sigma E'(2\rho\sigma)^{1/2}]$
m	=	combined mean absolute profile slope, m/m, $(m_1^2+m_2^2)^{1/2}$
P	=	contact pressure, N/m^2
P_{app}	=	apparent contact pressure, N/m^2
P_0	=	maximum contact pressure (at $r=0$) for rough spheres, N/m^2
$P_{0,\text{Hz}}$	=	Hertz maximum contact pressure (at $r=0$) for smooth spheres, N/m^2
P^*	=	dimensionless contact pressure, $P/[E'(\sigma/8\rho)^{1/2}]$
$R_{C,L}$	=	large-scale thermal contact resistance, m$^2\cdot$K/W
$R_{C,S}$	=	small-scale thermal contact resistance, m$^2\cdot$K/W
r	=	distance from center of axisymmetric contact, m
α	=	load redistribution parameter
δ	=	combined crown drop of surfaces, m, $\delta_1+\delta_2$
ζ_n	=	nth root of Bessel function $J_1(\zeta_n)$
ν	=	Poisson ratio
ρ	=	combined radius of curvature, m, $(1/\rho_1+1/\rho_2)^{-1}$
σ	=	combined rms roughness, m, $(\sigma_1^2+\sigma_2^2)^{1/2}$

Subscripts

C	=	contact
L	=	large-scale, macroscopic
n	=	index of summation
S	=	small-scale, microscopic
0	=	at axis or center of contact
1	=	specimen or surface 1
2	=	specimen or surface 2

I. Introduction

JUNCTION thermal conductance is important in many areas of engineering design. For example, the magnitude of conductance must be known to predict thermally induced stresses between the skin and structure of aerodynamically heated supersonic flight vehicles. The conductance between the radioactive fuel pellets and the metallic cladding in nuclear reactor fuel rods must be maximized to ensure safe operation. Electronic devices contain myriad junctions in the thermal circuit between the integrated circuits and ultimate heat sinks, and the thermal resistance of these junctions increases operating temperature, causing premature failure. In spacecraft and satellites, one of the primary modes of heat rejection is conduction from the payload to the radiators across a number of bolted joints. In gas-turbine engines, high conductance between the roots of the turbine blades and the internally air-cooled rotor shaft is essential.

Presented as Paper 98-2759 at the AIAA/ASME 7th Joint Thermophysics and Heat Transfer Conference, Albuquerque, NM, 15–18 June 1998; received 5 January 2005; revision received 12 January 2005; accepted for publication 22 January 2005.

*Assistant Professor, Department of Mechanical & Aerospace Engineering. Associate Fellow AIAA.
†Research Scientist. Member AIAA.
‡Thomas A. Dietz Professor, Department of Mechanical Engineering. Honorary Fellow and Past President AIAA.

Conversely, conductance through the insulation of cryogenic storage tanks should often be minimized.

Junction thermal conductance, h_{junc}, has three components: conduction and convection through fluid in the gaps between the contacting surfaces, h_g; radiation across the junction, h_{rad}; and conduction through contacts (or solid spots), h_c. For spacecraft, which operate in high-vacuum conditions, h_g is negligible. Except for cold plate connections utilizing parallel radiative fins, h_{rad} is also negligible. Thus, in some instances, contact (or solid spot) conductance, h_c, is the only mode by which heat is transferred across a junction.

Metals are employed almost exclusively in joints where maximum junction thermal conductance is desired. A number of theoretical and empirical models for predicting thermal contact conductance of metallic junctions have been published. Correlations by Cooper et al.,[1] Mikic,[2] and Yovanovich[3] yield accurate predictions of contact conductance for nearly optically flat (i.e., total nonflatness [*TIR*] less than 2 μm) rough metals. For the case of the opposite extreme geometry, namely, smooth, spherical surfaces, Clausing and Chao[4] derived a simple model, which they verified against experiments. However, in many practical applications, limits of metal-forming technology (machining, extruding, forging, etc.) in addition to mechanically and thermally induced warpage result in widely varying roughness and flatness.

Mikic and Rohsenow,[5] Thomas and Sayles,[6] and Burde and Yovanovich[7] addressed nonflat surfaces by assuming they are spherical and derived models for predicting contact conductance of spherical, rough metals. However, their models entail very intensive, sometimes iterative, computations. Making these models suitable for design studies would require encoding them in rather complex computer programs. Nishino et al.[8] combined the theory of Mikic,[9] which predicts contact conductance for a given nonuniform contact pressure distribution, with the mechanical/metrological models of Greenwood and Tripp,[10] Tsukada and Anno,[11] and Sasajima and Tsukada[12] for contacting rough spheres. Nishino et al.[8] verified their resultant model for thermal contact conductance of spherical, rough metals against experimental data. However, they did not demonstrate how to apply their model, thereby limiting its utility for design.

Lambert and Fletcher[13–15] developed a semi-empirical model to account for intermediate cases for which both roughness and nonflatness (sphericity) significantly influence contact conductance. Lambert and Fletcher[13] demonstrated the general robustness of their model in comparison to 1265 conductance results for 12 metals and alloys with widely ranging nonflatness and roughness, which they extracted from the literature. However, the model was not presented in a simple, graphical format.

Lambert and Fletcher[14,15] further verified the validity of their model and provided a complete description of how to utilize it. However, the many necessary calculations make the model very tedious for computations by hand. Hence, to facilitate rapid, easy estimations of conductance, Lambert and Fletcher[16] developed a set of graphical conductance solutions for contacts of six commonly used metals (stainless steel 304, copper, brass, aluminum alloy 6061-T6, magnesium alloy AZ31B, and titanium alloy Ti-6Al-4V). Lambert and Fletcher[16] also eliminated two of the three empirical polynomial correction factors (f_S and g) present in the original model[13–15] at the expense of a minor loss in accuracy.

In the present work, the model is extended to dissimilar contacts of the same three light alloys (aluminum alloy 6061-T6, magnesium alloy AZ31B, and titanium alloy Ti-6Al-4V) treated by Lambert and Fletcher.[16] Furthermore, in the present investigation, the model has been thoroughly reanalyzed, resulting in improved accuracy and the jettisoning of the third and final empirical correction factor (f_L). Thus, the present form of the model is unencumbered by nonphysically based correction terms, making it much more elegant (and inherently more acceptable) than its predecessor.

The present model allows the engineer to quickly and easily estimate thermal contact conductance of metallic junctions with the following information: type(s) of metal or alloy, apparent contact pressure, and geometry (size, nonflatness, and roughness) of the contacting surfaces. Results are provided for similar and dissimilar pairs of three light alloys often used in aerospace applications: aluminum alloy 6061-T6, magnesium alloy AZ31B, and titanium alloy Ti-6Al-4V.

II. Model Development

A. Assumptions of the Present Model

1) Contacting surfaces are circular, macroscopically spherical (see Sec. II.B for the underlying rationale), and microscopically rough with a Gaussian height distribution.

2) Contact microhardness, H_C, is determined from Vickers microhardness, H_V, and σ/m according to the method developed by Hegazy.[17] In practice, H_C is approximated as H_V or Knoop microhardness, H_K.

3) Heat flows only through solid contacts; that is, gap fluid conductance and radiative heat transfer are negligible.

4) Thermal rectification is not considered. This is the phenomenon in which conductance is greater in one direction than in the other, due to either dissimilar materials or roughness.

B. Selection of Spherical Macroscopic Surface Profile

A universal model capable of dealing with completely arbitrary surface profiles would probably be overly cumbersome at best, if not intractable. Wide applicability need not be sacrificed in the interest of simplifying the model. It is assumed herein that the macroscopic topography can be described by one or a few parameters, just as the microscopic topography is described quite well by combined rms roughness, σ, and combined mean absolute profile slope, m. A sphere is the simplest example, because its macroscopic profile is completely described by one parameter: its radius of curvature, ρ. This geometry is illustrated in Fig. 1.

Clausing and Chao,[4] Mikic and Rohsenow,[5] and Nishino et al.,[8] among others, also used this simplification. This assumption is often justifiable, because nominally flat surfaces are often contoured spherical, or at least are quite often crowned (convex) with monotonic curvature in at least one direction. This last observation is based on the authors' examination of surface profiles for the contact surfaces (ends) of dozens of cylindrical samples used in contact conductance tests. The ends of these samples were finished by various

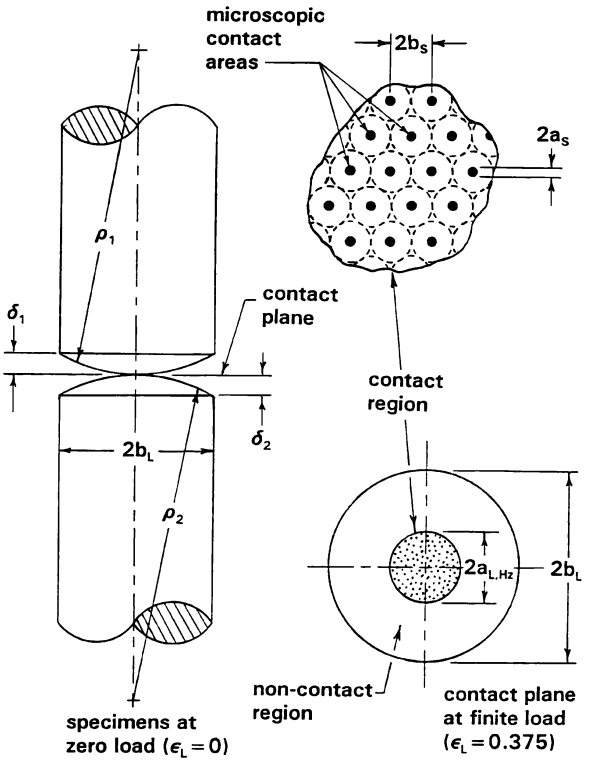

Fig. 1 Contacting spherical, rough surfaces showing the macroscopic contact radius, $a_{L,\text{Hz}}$, predicted by Hertz.[18] Note that $a_{L,\text{Hz}} \leq a_L$. Also shown is an idealized array of microcontacts.

methods: turning, grinding, and lapping. The last method, lapping, employed a special fixture to prevent wobbling of the samples, which invariably occurred during grinding and which resulted in crowned surfaces.

C. Thermal Contact Resistance Model of Mikic[9]

Mikic[9] traces the development of expressions for the total (microscopic, $R_{C,S}$, plus macroscopic, $R_{C,L}$) thermal contact resistance resulting from a nonuniform, axisymmetric contact pressure distribution [$P = P(r)$], and these are given in the following. It does not address how to determine the pressure distribution, and this remains the crux of the problem:

$$R_{C,S} = 0.345\frac{\sigma}{km}\left[\int_0^1 \frac{r}{b_L}\left(\frac{P}{H_C}\right)^{0.985} d\left(\frac{r}{b_L}\right)\right]^{-1} \tag{1}$$

$$R_{C,L} = 8\frac{b_L}{k}\sum_{n=1}^{\infty}\frac{\left[\int_0^1 (r/b_L)(P/P_{\text{app}})^{0.985} J_0[\zeta_n(r/b_L)]d(r/b_L)\right]^2}{\zeta_n J_0^2(\zeta_n)} \tag{2}$$

D. Pressure Distribution for Contact of Elastic, Rough Spheres

Greenwood and Tripp[10] developed a contact model for the elastic deformation of rough spheres. For applications where thermal contact conductance is relevant, contact loads are usually of such magnitude so as to cause only macroscopic elastic deformation. They introduced the following two dimensionless variables:

$$L^* = 2L\Big/\sigma E'\sqrt{2\rho\sigma} \tag{3}$$

$$P^* = P\Big/E'\sqrt{\sigma/8\rho} \tag{4}$$

where P^* and L^* are the dimensionless pressure and dimensionless load, respectively. The definition of P^* is not rigorously defined by Greenwood and Tripp[10] to be either the local, average, or apparent contact pressure. The definition of dimensionless load, L^*, however, is straightforward, because L is merely the contact load. The correlation developed herein utilizes L^*.

Hertz[18] developed a model for the pressure distribution and contact spot radius for two contacting, perfectly smooth, elastic spheres. For a given load, increasing the ratio of roughness to radius of curvature, σ/ρ, from zero (for a perfectly smooth sphere) causes an enlargement of the contact region and a reduction in the intensity of the contact pressure with respect to the Hertz[18] solution. Sasajima and Tsukada[12] defined two dimensionless ratios to characterize this behavior. $P_0/P_{0,\text{Hz}}$ is the ratio of actual contact pressure (for rough spheres) to the contact pressure predicted by Hertz[18] (for smooth spheres) at the center of contact (at $r = 0$, where pressure is greatest); $a_L/a_{L,\text{Hz}}$ is the actual macroscopic contact radius over the contact radius predicted by Hertz.[18] Tsukada and Anno[11] and Sasajima and Tsukada[12] give experimental and computed values of $P_0/P_{0,\text{Hz}}$ for $L^* > 0.1$, that is, contacts for which sphericity is more pronounced. The model by Greenwood and Tripp[10] was used to extrapolate values of $P_0/P_{0,\text{Hz}}$ for $L^* < 0.1$, as shown in Fig. 2. $P_0/P_{0,\text{Hz}}$is expressed by

$$P_0/P_{0,\text{Hz}} = (1/\{1 + 1/[0.3585 \times (L^*)^{0.5840}]^{1.11}\})^{1/1.11} \tag{5}$$

Sasajima and Tsukada[12] developed an expression for contact pressure as a function of radial distance from the center of contact:

$$P(r) = P_0\left[1 - (r/a_L)^2\right]^{\alpha} \tag{6}$$

The exponent α is 1 for smooth spheres (large L^*) and is greater than 1 for rough spheres (small L^*) and asymptotically approaches 3. It is given by

$$\alpha = 2 - \tanh[\log(L^*) - 1.8] \tag{7}$$

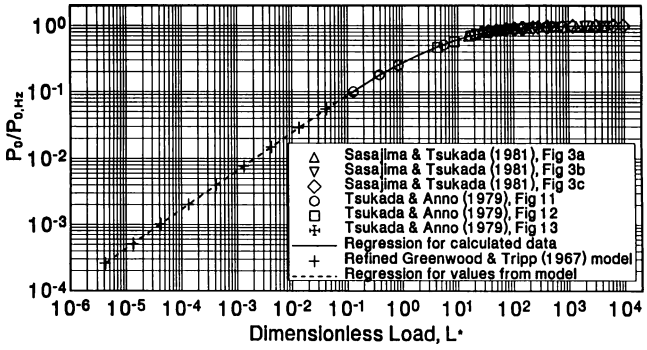

Fig. 2 Ratio of peak ($r = 0$) contact pressure $P_0/P_{0,\text{Hz}}$ for rough and smooth spheres.

The ratio of the actual macroscopic contact radius (for rough spheres) to the Hertz[18] macroscopic contact radius (for smooth spheres), $a_L/a_{L,\text{Hz}}$, is computed from $P_0/P_{0,\text{Hz}}$ and α:

$$\frac{a_L}{a_{L,\text{Hz}}} = \left[\frac{2(\alpha+1)}{3(P_0/P_{0,\text{Hz}})}\right]^{\frac{1}{2}} \tag{8}$$

The term b_L/a_L is the ratio of the surface radius to the actual macroscopic contact radius:

$$b_L/a_L = b_L/(a_L/a_{L,\text{Hz}})a_{L,\text{Hz}} = b_L/(a_L/a_{L,\text{Hz}})(3L\rho/4E')^{\frac{1}{3}} \tag{9}$$

E. Model for Thermal Contact Conductance of Spherical, Rough Metals

The present model was obtained by using the aforementioned contact model to define the pressure distribution, $P(r)$, in terms of load, mechanical properties, and surface geometry. $P(r)$ was then substituted into Eqs. (1) and (2) by Mikic[9] for $R_{C,S}$ and $R_{C,L}$.

Buckingham Pi dimensional analysis was employed to determine the effect of each physical parameter on $R_{C,S}$ and $R_{C,L}$. This resulted in the following correlations:

$$R_{C,S} = \frac{6.15(L^*)^{0.484}(b_L/a_L)^2}{(km/\sigma)(L/H_C\rho\sigma)^{0.95}(P_0/P_{0,\text{Hz}})^{0.67}} \tag{10}$$

$$R_{C,L} = \frac{1.44(L^*)^{0.954}(P_0/P_{0,\text{Hz}})^{0.20}(b_L/a_L)^2}{(kL/\rho\sigma^2E')} \tag{11}$$

Equations (10) and (11) contain $P_0/P_{0,\text{Hz}}$ raised to different powers. This was required to linearize both $R_{C,S}$ and $R_{C,L}$ in terms of L^*, so that they could be expressed as power-law regressions. Thermal contact conductance, $h_{C,S+L}$, is obtained from $R_{C,S}$ and $R_{C,L}$ by

$$h_{C,S+L} = 1/(R_{C,S} + R_{C,L}) \tag{12}$$

The predictive correlations for $R_{C,S}$ and $R_{C,L}$ are applicable for any conceivable range of conditions. The dimensionless load L^* was varied from 4.2×10^{-5} (i.e., essentially optically flat for any realistically sized component) up to 1.3×10^4 (i.e., a smooth sphere for all practical purposes). The ratio b_L/a_L was varied from 10^{-4} up to 10^3. This covers the range of possibilities from an almost perfectly uniform pressure, where only the very center of the predicted $P(r)$ is actually brought to bear on the surfaces to a very small contact on a very large surface, say, $a_L = 1$ mm and $b_L = 1.0$ m. However, for the wide range of surface measurements considered herein, which encompass nearly all likely practical situations, b_L/a_L varied between 1×10^{-1} and 2.53×10^{-1}.

F. Estimation of Unspecified Parameters

Mean absolute profile slope, m, was provided in few experimental investigations performed in the 1960s and 1970s and is often not known or specified in design studies. Lambert and Fletcher[13] observed a definite, statistically significant trend between m and σ in those data reported in the literature and in the dozens of surfaces

they characterized. They correlated m to σ for experiments in which both parameters were listed:

$$m_{1or2} = 0.076\sqrt{\sigma_{1or2} \times 10^6} \tag{13}$$

Uncertainty in this empirical correlation may, in extreme cases, be plus or minus a factor of 2. However, profilometers capable of determining m are being used more and more in the electronics and spacecraft industries, and so estimation of m should no longer be necessary.

Also, experimental studies rarely list the radii of curvature, ρ_1 and ρ_2, of the specimen surfaces. To circumvent this difficulty, the combined radius of curvature, ρ, may be estimated from the combined nonflatness, *TIR*. In the present study, the combined crown drop, δ, is assumed to equal *TIR* (see Fig. 1). Thus, ρ is

$$\rho = b_L^2 \big/ 2\delta \tag{14}$$

The concept of radius of curvature loses relevance if the surfaces are decidedly nonspherical. If this is so, the present model may substantially disagree (typically in an overly conservative fashion) with experimental data, but usually by no more than a factor of 3, as evidenced by comparison to experimental data.

For noncircular specimens, an effective macroscopic contact radius b'_L is defined as

$$b'_L = \sqrt{A_{\text{app}}/\pi} \tag{15}$$

This expression is useful for commonly utilized square or rectangular surfaces (provided the length is not, say, more than twice the width for rectangular surfaces) or less-frequently encountered triangular surfaces (approximately equilateral). This method of estimating b_L for noncircular contact surfaces is supported by Yovanovich et al.[19]

G. Generation of Design Graphs for Thermal Contact Conductance

The present simplified and improved model of Lambert and Fletcher,[13–16] as described and developed earlier, was used to generate plots of thermal contact conductance for similar and dissimilar contacts of three light structural alloys of interest in aerospace applications. These are aluminum alloy 6061-T6, magnesium alloy AZ31B, and titanium alloy Ti-6Al-4V. Their relevant physical properties at room temperature, 300 K, are listed in Table 1.

Conductance values were calculated for three surface radii, $b_L = 1$, 3, and 10 cm, representative of small, medium, and large surfaces, respectively (see Table 2). Crown drop δ and roughness σ span the ranges conceivably encountered in practice. Apparent contact pressure, P_{app}, was varied from very light (10 kPa = 1.45 psi) to very intense (100 MPa = 14,500 psi).

Graphs of thermal contact conductance were generated for the material combinations shown in Table 3.

Table 1 Physical properties of three light alloys at 300 K

Metal/alloy	k, W/m · K	E, GPa	ν	H_C, MPa
Aluminum alloy 6061-T6	181	69	0.33	930
Magnesium alloy AZ31B	87	45	0.35	510
Titanium alloy Ti-6Al-4V	6.7	114	0.342	3820

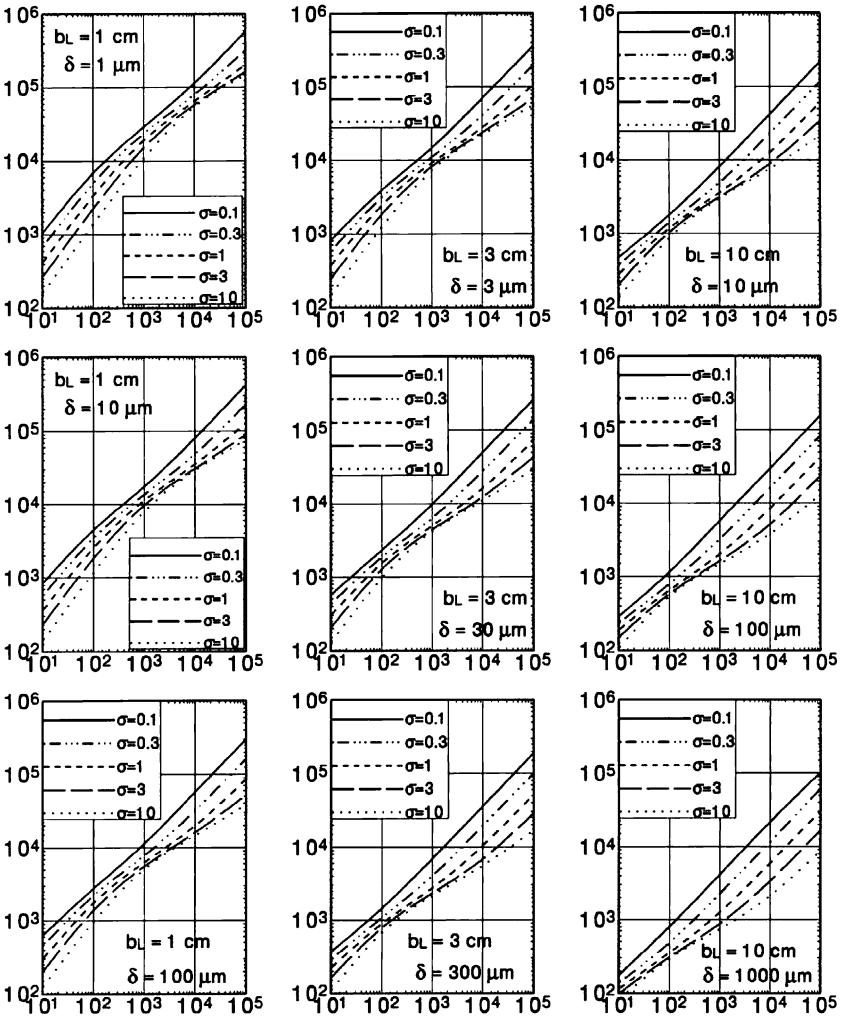

Fig. 3 Thermal contact conductance graphs at 300 K for aluminum alloy 6061-T6/aluminum alloy 6061-T6, magnesium alloy AZ31B/magnesium alloy AZ31B, aluminum alloy 6061-T6/magnesium alloy AZ31B; abscissa: apparent contact pressure, P_{app} (kPa); ordinate: thermal contact conductance, $h_{c,S+L}$ (W/m^2 · K); σ = roughness (μm); δ = crown drop (μm); b_L = radius of surface (cm).

H. Utilizing Conductance Graphs for Design

Figures 3 through 5 are graphical solutions for thermal contact conductance of the metal combinations in Table 3 over the ranges of geometrical and load parameters listed in Table 2.

To utilize Figs. 3–5 for a known combination of material(s), geometry, and load, one proceeds directly to the appropriate figure. To determine which material(s), pressure, and dimensions are appropriate to achieve a desired conductance, one may temporarily select an alloy pair and an allowable apparent contact pressure, P_{app}, and then proceed to the figure for the chosen alloy pair and determine what combination(s) of geometrical parameters are appropriate.

Table 2 Geometrical and load parameters

b_L, cm	δ, μm	σ, μm	P_{app}, KPa
1	1, 10, 100	0.1, 0.3, 1, 3, 10	10^1–10^5
3	3, 30, 300	0.1, 0.3, 1, 3, 10	10^1–10^5
10	10, 100, 1000	0.1, 0.3, 1, 3, 10	10^1–10^5

Table 3 Similar and dissimilar contact pairs

Figure	Combination
3	Aluminum alloy 6061-T6 ↔ Aluminum alloy 6061-T6
	Magnesium alloy AZ31B ↔ Magnesium alloy AZ31B
	Aluminum alloy 6061-T6 ↔ Magnesium alloy AZ31B
4	Titanium alloy Ti-6Al-4V ↔ Titanium alloy Ti-6Al-4V
5	Aluminum alloy 6061-T6 ↔ Titanium alloy Ti-6Al-4V
	Magnesium alloy AZ31B ↔ Titanium alloy Ti-6Al-4V

The graphs provide estimates of conductance for freshly machined surfaces with minimal oxidation. Aluminum and magnesium alloys oxidize readily in air. A thin oxide layer also forms on titanium alloys exposed to air. In fact, an oxide layer begins to form on these metals immediately after machining. (Brass, copper, and stainless steel also oxidize in air at varying rates.)

Oxidation increases microscopic thermal contact resistance, $R_{C,S}$, which predominates for relatively flat, rough surfaces. Lambert[13] determined empirically that lightly oxidized aluminum, magnesium, and copper, in relatively new contacts not exposed to excessive moisture and salt spray, exhibit $R_{C,S}$ magnitudes some three times greater than predicted values (i.e., for freshly machined surfaces). For old contacts and those subjected to harsh environments, the $R_{C,S}$ values of aluminum, magnesium, and copper are some 10 times greater than predicted magnitudes. Thus, for relatively flat, rough surfaces for which δ/σ less than, say, 10, the conductance values should be reduced by a factor of 3 to 10 depending on the duration and severity of service.

The authors concede that this predictive tool is far from exact. But the correlation, its attendant graphs, and the aforementioned method of dealing with oxidation should be viewed as a means of obtaining conservative estimates of contact conductance to provide engineers with a level of confidence in employing this model in design.

III. Experimental Program

A. Apparatus and Specimens

Few well-characterized data on contact conductance of dissimilar pairs of aluminum, magnesium, and titanium alloys suitable for comparison to the model were located in the literature. Hence, it was decided to obtain new experimental results for comparison.

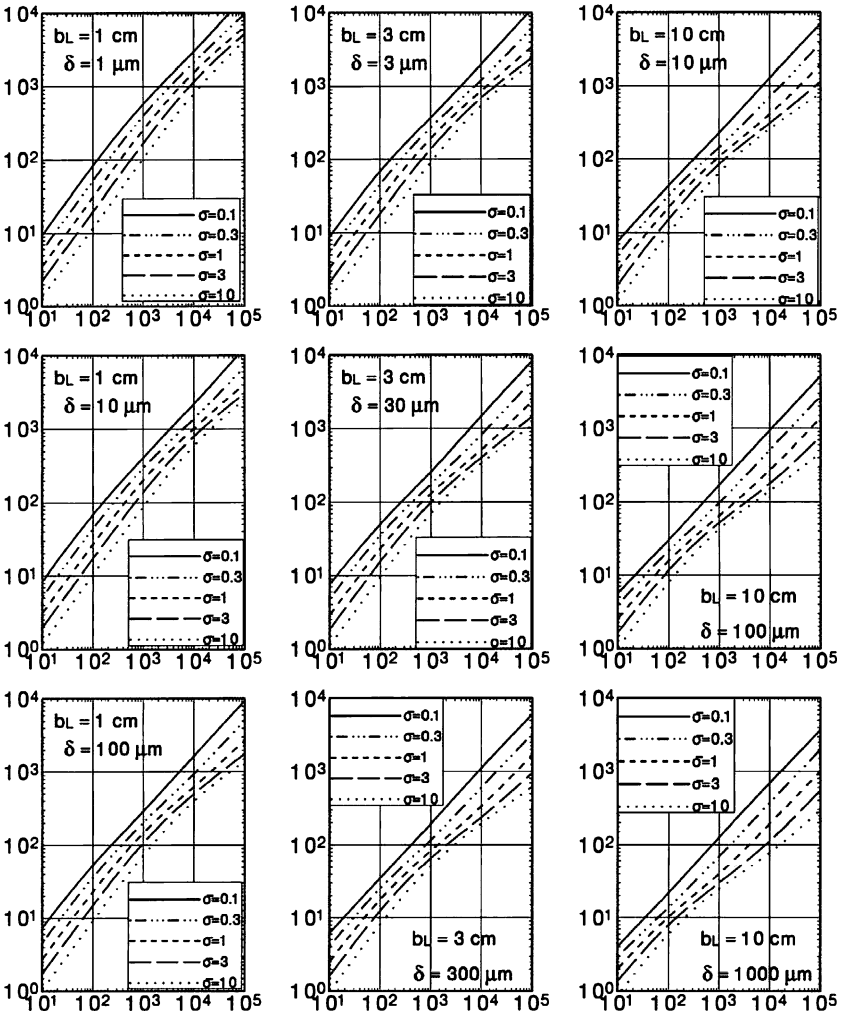

Fig. 4 Thermal contact conductance graphs at 300 K for titanium alloy Ti-6Al-4V/titanium alloy Ti-6Al-4V; abscissa: apparent contact pressure, P_{app} (kPa); ordinate: thermal contact conductance, $h_{c,S+L}$ (W/m^2 · K); σ = roughness (μm); δ = crown drop (μm); b_L = radius of surface (cm).

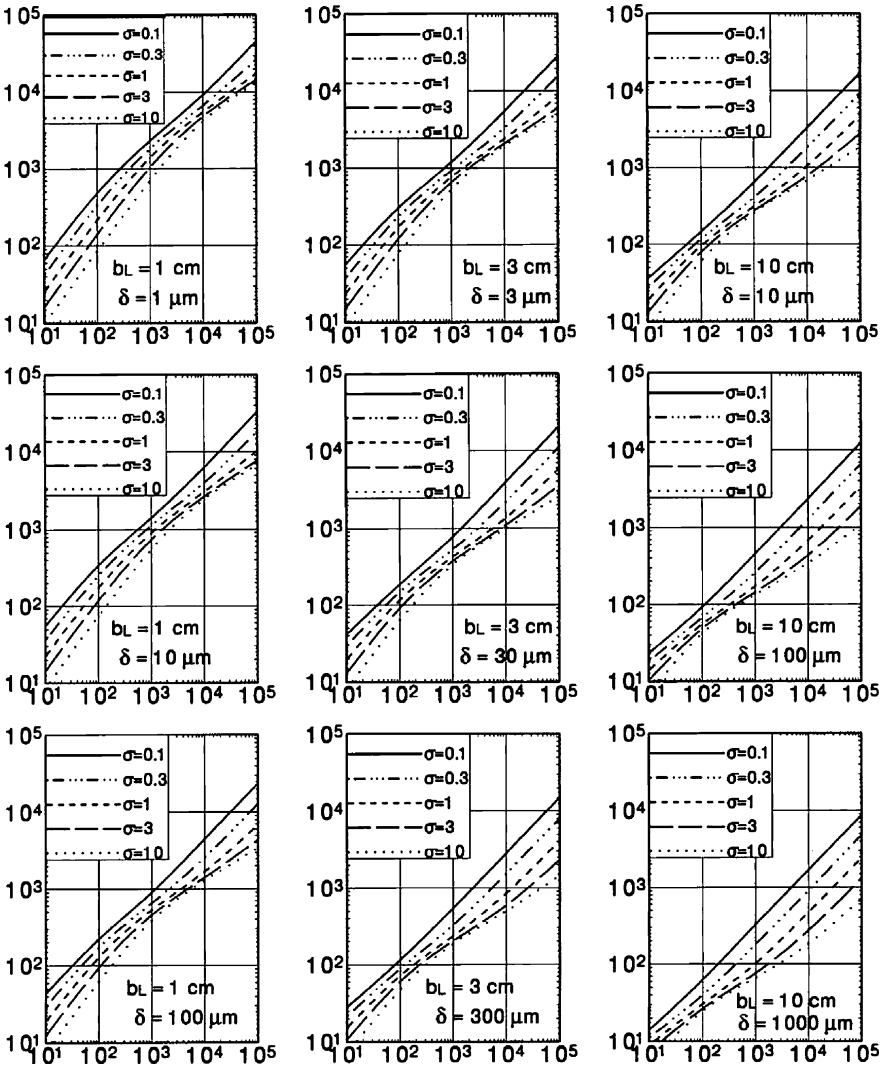

Fig. 5 Thermal contact conductance graphs at 300 K for aluminum alloy 6061-T6/titanium alloy Ti-6Al-4V; magnesium alloy AZ31B/titanium alloy Ti-6Al-4V; abscissa: apparent contact pressure, P_{app} (kPa); ordinate: thermal contact conductance, $h_{c,S+L}$ (W/m^2 · K); σ = roughness (μm); δ = crown drop (μm); b_L = radius of surface (cm).

The experimental apparatus (Fig. 6) employs the standard, cut bar technique for determining contact conductance. It is composed of a load frame, which supports two heat sources/sinks into which the cylindrical upper and lower heat flux meters are inserted. A cylindrical specimen is inserted between the upper and lower heat flux meters. Pressurized bellows and a load cell are used to control and measure the load on the contact interface. Large ball bearings are used to transmit load from the frame through the test column to ensure uniform loading of the contact interfaces. The facility is enclosed in a vacuum chamber to reduce convective losses to a negligible level. Each specimen and heat flux meter is 2.54 cm (1.00 in.) in diameter and is instrumented with five type K (chromel–alumel) thermocouples inserted into holes drilled to their axes at 6.35-mm (0.25-in.) intervals.

Heat flux is determined from Fourier's law, the predetermined conductivity of the sample materials, and the measured temperature gradients in the samples. Contact conductance is computed from the heat flux and the temperature drop across the junction, which is obtained by extrapolating the temperature gradients in the samples to the interface.

For the present investigation, three nominal values of crown drop δ (8, 20, and 200 μm) were employed with roughness ranging from 0.21 to 0.32 μm. Apparent contact pressure was increased from 172 to 4137 kPa (25 to 600 psi) after a preload to the maximum pressure, whereas mean interface temperature was maintained at 25°C.

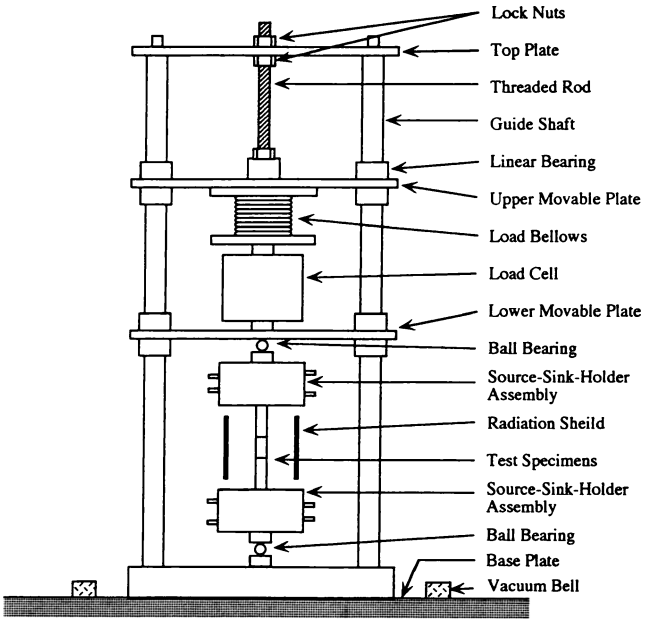

Fig. 6 Experimental apparatus.

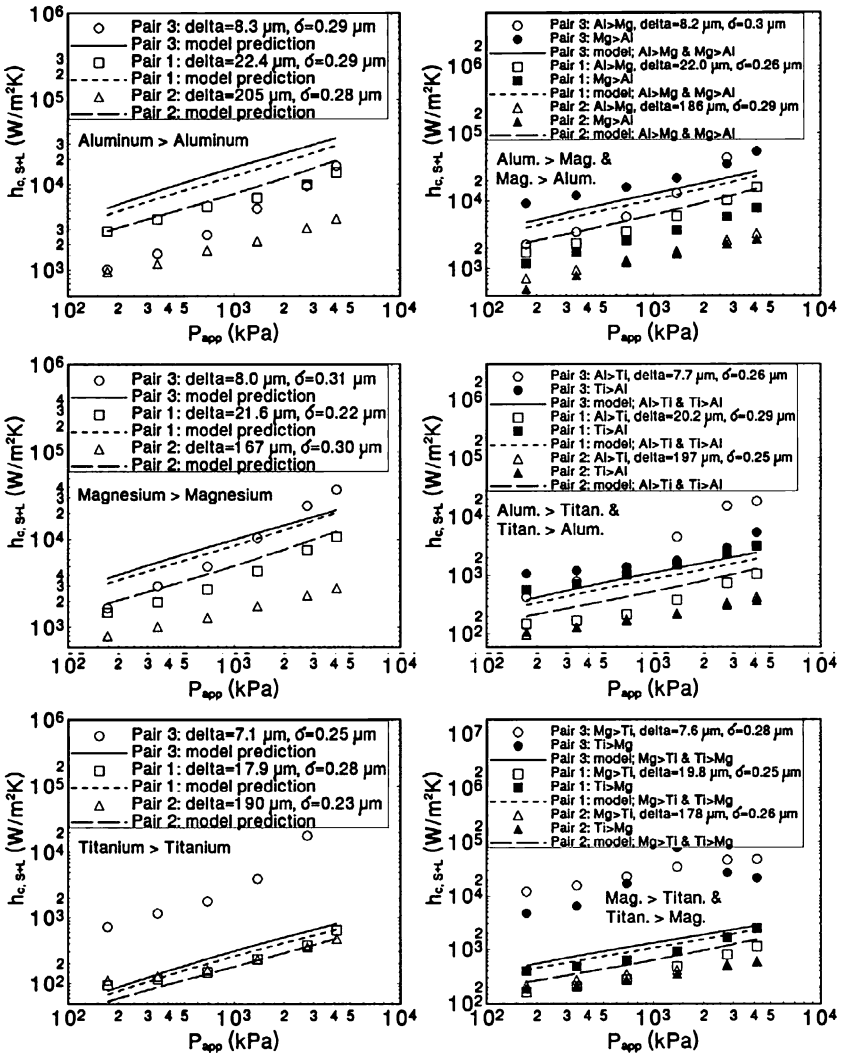

Fig. 7 Comparison of model to experiments for similar and dissimilar contacts of aluminum alloy 6061-T6, magnesium alloy AZ31B, and titanium alloy Ti-6Al-4V.

B. Comparison Between Model and Experiment

Experimental results for the six possible combinations (see Table 3) of the three selected alloys (aluminum alloy 6061-T6, magnesium alloy AZ31B, and titanium alloy Ti-6Al-4V) are compared to the present model in Fig. 7.

As expected, the experimental results for most contacts involving similar and dissimilar contacts of aluminum and magnesium are 3 to 10 times lower than the model predictions. This is due to oxidation of the surfaces.

Very flat contacts involving titanium produced results as much as an order of magnitude greater than the model. This was determined to be due to high uncertainties in the experiments. Very small heat fluxes were required to maintain an interface temperature of 25°C for contacts involving titanium, because of its very low thermal conductivity (half that of stainless steel 304). Such low heat fluxes resulted in junction temperature differences that were often too small to be accurately measured.

IV. Conclusions

Figures 3–5 provide a simple, graphical method for estimating thermal contact conductance of similar and dissimilar pairings of three commonly used aerospace alloys, aluminum alloy 6061-T6, magnesium alloy AZ31B, and titanium alloy Ti-6Al-4V. This graphical technique expedites parametric design studies and enables rapid cost–benefit analysis of how changing a particular surface measurement (or nominal contact pressure) will affect thermal contact conductance.

Acknowledgments

The authors thank M. M. Yovanovich of the Department of Mechanical Engineering at the University of Waterloo, Ontario, for graciously providing the simple yet elegant and accurate correlation for $P_0/P_{0,\mathrm{Hz}}$ vs L^* [Eq. (5)].

References

[1]Cooper, M., Mikic, B. B., and Yovanovich, M. M., "Thermal Contact Conductance," *International Journal of Heat and Mass Transfer*, Vol. 12, No. 2, 1969, pp. 279–300.

[2]Mikic, B. B., "Thermal Contact Conductance; Theoretical Considerations," *International Journal of Heat and Mass Transfer*, Vol. 17, No. 1, 1974, pp. 205–214.

[3]Yovanovich, M. M., "Thermal Contact Correlations," *Spacecraft Radiative Transfer and Temperature Control*, edited by T. E. Horton, Progress in Aeronautics and Astronautics, Vol. 83, AIAA, Washington, DC, 1982, pp. 83–95.

[4]Clausing, A. M., and Chao, B. T., "Thermal Contact Resistance in a Vacuum Environment," *Journal of Heat Transfer*, Vol. 87, No. 3, 1965, pp. 243–251.

[5]Mikic, B. B., and Rohsenow, W. M., "Thermal Contact Conductance," Technical Rept. 4542-41, Dept. of Mechanical Engineering, Massachusetts Inst. of Technology, Cambridge, MA, Sept. 1966.

[6]Thomas, T. R., and Sayles, R. S., "Random-Process Analysis of the Effect of Waviness on Thermal Contact Resistance," AIAA Paper 74-691, July 1974.

[7]Burde, S. S., and Yovanovich, M. M., "Thermal Resistance at Smooth-Sphere/Rough-Flat Contacts: Theoretical Analysis," *Progress in Astronautics and Aeronautics, Thermophysics and Thermal Control*, Vol. 65, 1978, pp. 83–102.

[8]Nishino, K., Yamashita, S., and Torii, K., "Thermal Contact Conductance Under Low Applied Load in a Vacuum Environment," *Proceedings of the First International Conference of Aerospace Heat Exchanger Technology*, edited by R. K. Shah and A. Hashemi, Elsevier, Amsterdam, 1993, pp. 763–788.

[9]Mikic, B. B., "Thermal Constriction Resistance Due to Non-Uniform Surface Conditions; Contact Resistance at Non-Uniform Interface Pressure," *International Journal of Heat and Mass Transfer*, Vol. 13, No. 8, 1970, pp. 1497–1500.

[10]Greenwood, J. A., and Tripp, J. H., "The Elastic Contact of Rough Spheres," *Journal of Applied Mechanics*, Vol. 89, No. 1, 1967, pp. 153–159.

[11]Tsukada, T., and Anno, Y., "On the Approach Between a Sphere and a Rough Surface (1st Report, Analysis of Contact Radius and Interface Pressure)," *Journal of the Japanese Society of Precision Engineering*, Vol. 45, No. 4, 1979, pp. 473–479.

[12]Sasajima, K., and Tsukada, T., "On the Approach Between a Sphere and a Rough Surface (2nd Report, Critical Condition to Yield Plastic Deformation in Contacting Bodies," *Journal of the Japanese Society of Precision Engineering*, Vol. 47, No. 6, 1981, pp. 694–699.

[13]Lambert, M. A., and Fletcher, L. S., "Thermal Contact Conductance of Non-Flat, Rough Metals in Vacuum," 4th ASME/JSME Joint Thermal Engineering Conf., American Society of Mechanical Engineers, New York, March 1995.

[14]Lambert, M. A., and Fletcher, L. S., "Thermal Contact Conductance of Spherical, Rough Metals," American Society of Mechanical Engineers, Heat Transfer Division, New York, Vol. 327, 1996, pp. 169–175.

[15]Lambert, M. A., and Fletcher, L. S., "Thermal Contact Conductance of Spherical, Rough Metals," *Journal of Heat Transfer*, Vol. 119, No. 4, 1997, pp. 684–690.

[16]Lambert, M. A., and Fletcher, L. S., "Design Graphs for Thermal Contact Conductance of Metals," AIAA Paper 97-2462, June 1997.

[17]Hegazy, A. A., "Thermal Joint Conductance of Conforming Rough Surfaces," Ph.D. Dissertation, Dept. of Mechanical Engineering, Univ. of Waterloo, Waterloo, Ontario, Canada, 1985.

[18]Hertz, H. R., *Miscellaneous Papers*, English Trans., MacMillan, London, 1896.

[19]Yovanovich, M. M., Burde, S. S., and Thompson, J. C., "Thermal Constriction Resistance of Arbitrary Planar Contacts with Constant Flux," *Thermophysics of Spacecraft and Outer Planet Entry Control*, edited by A. M. Smith, Progress in Aeronautics and Astronautics, Vol. 56, AIAA, Washington, DC, 1977, pp. 127–140.